THE JOURNAL OF PHYSICAL CHEMISTRY B

Article

pubs.acs.org/JPCB

Simulations of Potentials of Mean Force for Separating a Leucine Zipper Dimer and the Basic Region of a Basic Region Leucine Zipper Dimer

Robert I. Cukier*

Department of Chemistry, Michigan State University, East Lansing, Michigan 48824-1322, United States

ABSTRACT: Basic region leucine zipper (bZIP) transcription factors involved in DNA recognition are dimeric proteins. The monomers consist of two subdomains, a leucine zipper sequence responsible for dimerization and a highly basic DNA recognition sequence. Leucine zippers are strongly dimerized, and in a bZIP, the basic region can, in the absence of DNA, undergo extensive relative monomer-to-monomer fluctuations. In this work, LZ and bZIP potentials of mean force (PMFs), which provide free energies along reaction coordinates, are simulated with a distance replica exchange method. The method uses restraint potentials to provide sampling along a reaction coordinate and enhances configuration space exploration by exchanging information between neighboring restraint potential configurations. Restraint potentials that are constructed from sums over a number of atom distances are employed. Their use requires a modification of the Weighted Histogram Analysis Method (WHAM) procedure to combine and unbias the data from the different restraint-potential-biased window densities to provide a PMF. These methods are first used to obtain a PMF for separating a leucine zipper (GCN4-p1) of the yeast transcriptional activator GCN4. The PMF indicates a very strong binding free energy that only weakens when the monomers are separated by about 12 Å, which is about 6 Å beyond their bound, dimer equilibrium distance. PMFs are also obtained for separating the basic subdomain monomer parts of the GCN4 bZIP transcriptional factor, in the absence of DNA. In a monomer separation range spanning the open, crystal-based structure to closer configurations, the basic subdomain PMF is quite flat, implying essentially thermal sampling in this distance range. A PMF generated starting from a "collapsed" state, taken from a previous simulation (*J. Phys. Chem. B* **2012**, *116*, 6071), where collapsed refers to the feature that the basic subdomain monomers are also effectively dimerized, shows that this state is bound in free energy, though much less so than the leucine zipper dimer.

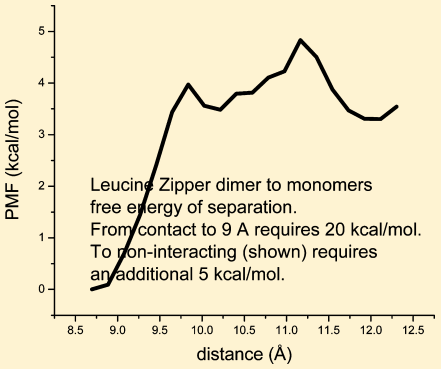

1. INTRODUCTION

A number of DNA binding transcription factors are formed by dimerization of monomeric proteins.[1] The basic region leucine zipper (bZIP) transcriptional regulator superfamily aids in the regulation of development and metabolism and is seminal to other cell functions.[2,3] Different subdomains of bZIP are responsible for dimerization and DNA recognition.[4] Dimerization is the responsibility of a leucine zipper (LZ) sequence, producing a stable α-helical, coiled coil subdomain. Extensions of the LZ monomers that have a great excess of basic residues (referred to as the basic region) form a DNA recognition subdomain.

LZs,[5,6] generically, n repeating residue heptads $(abcdefg)n$, are examples of coiled coils and form an important class of structural motifs.[7−14] The LZ (GCN4-p1) that comprises the dimerization domain of the DNA-binding bZIP protein GCN4 is an α-helical, parallel, double-stranded coiled coil. The folding pathways and stability of GCN4-p1 and various mutants have been studied by experimental methods such as calorimetry, circular dichroism (CD), kinetics, hydrogen exchange, and NMR[12,13,15−19] and have been computationally addressed using lattice models,[20−23] coarse-grained models,[24] implicit solvent,[25,26] and explicit solvent[27−29] simulations.

In this work, aspects of the stability of the GCN4-p1 LZ and the GCN4 bZIP basic region subdomains are studied, motivated in part by some observations from our previous simulations. One focus of attention arises from the strong forces forming the LZ. The LZ dimer is very stable.[14,30] This stability was evident in our previous melting curve simulations[31] and from the spontaneous re-formation of the dimer from monomers that were relatively well-separated initially.[32] Here, we obtain a potential of mean force (PMF) for the initial stage (not to infinity) of separation of the dimer and find that to do so requires some new methodology.

In a bZIP, the net negatively charged DNA will interact with the basic region to form a stable complex. In the absence of DNA, the repulsion of the basic region monomers can lead to a sampling of a wide range of conformations, as shown by solution NMR and CD studies,[33−38] with some preference for helical conformations. In other, heterodimeric, bZIPs, the basic region of one monomer was found to be α-helical.[39] Thus, a

Received: May 13, 2014
Revised: July 21, 2014
Published: August 14, 2014

bZIP can be characterized as a stable α-helical coiled coil with basic regions that fluctuate around α-helical monomers.

Our previous bZIP simulation[40] in the absence of DNA showed that again, as a consequence of the strong forces, the LZ subdomain stays well dimerized, but the basic region was found to extensively fluctuate. In particular, dependent upon the particular MD run and the conditions of temperature and ionic strength, a scissor-like relative motion of the two basic region monomers occurred, with little impediment to the motion. However, for some trajectories, a "collapsed state" whereby the two monomers of the basic region also can be considered to be dimerized was found. In this state, the two basic region monomers approach each other to an interaction distance. It should be noted that while the basic region monomers have a net excess of positive charge, they have numerous negatively charged residues too, offering the possibility of monomer−monomer interactions. Here, too, a PMF, now for the relative basic region monomer separation, is of interest.

When a reaction coordinate, R, can be postulated, window methods are appropriate to obtain a PMF(R).[41,42] If window restraint potentials are introduced that are sufficiently strong to provide good sampling in the desired ranges of the reaction coordinate but are sufficiently weak to provide reasonable overlap of the histograms of the biased window distributions, then methods such as Weighted Histogram Analysis Method (WHAM)[43−46] can be used to unbias the pool of data from the windows, and the probability $p(R)$ of finding the reaction coordinate and the corresponding PMF(R) = $-k_BT \ln p(R)$ around R can be obtained. In principle, a sufficient number of windows can be used to satisfy both requirements, but that may prove to be too computationally expensive. An improvement on window methods is to use a variant[47] of the Replica Exchange Method (REM) that we shall refer to as distance REM (DREM).[31,48] As in any REM, in DREM, independently running MD replicas are interrupted periodically with attempts at exchanging neighbor data, here the window restraint potential values. Attempted exchanges are accepted/rejected according to the Metropolis Monte Carlo (MC) rule. DREM should enhance the exploration of configuration space by in effect introducing larger configuration changes when a move is accepted than the typical MD step does. In previous work, we have shown that DREM can greatly accelerate the exploration of configuration space relative to using the corresponding window method.[31,48] Another virtue of DREM is that the information from all of the windows is of use. That is in contrast to, for example, temperature REM, where typically only information about the ambient temperature replica is of interest.

In this work, we introduce a modification of the DREM to incorporate restraint potentials that are formed from the sum over a number of atom-to-atom distances. That will prove to be useful for the PMFs generated in this work. Note that the restraint is in the total potential; thus, it is a one-dimensional restraint. However, now the connection between the potential and restraint distance no longer is one-to-one, as is the case for a single restraint coordinate distance. Then, another method to judge the overlap of windows is required and developed herein. Also, the WHAM procedure must be done in two stages, one to obtain the biasing free energies and another to use them along with the biased window densities to obtain the PMF. The utility of this class of restraint potentials becomes evident in separating the LZ dimer. In particular, a restraint potential that involves monomer-to-monomer distances spread along the monomer axes serves to limit the relative monomer conformational space exploration. Similar considerations are also useful for the basic region PMF of bZIP.

The rest of the paper is organized as follows. Section 2 reviews the DREM protocol along with the new restraint potential and how to use and validate WHAM with this restraint potential. Specifics of the restraint potentials for the LZ and bZIP DREM simulations are presented. Sections 3 and 4 provide, respectively, the PMFs for the LZ and for the bZIP, along with details of how the DREM is performing. Section 5 provides a discussion of the PMFs and why some are readily determined while others require more extensive simulations. Appendix A considers a strong restraint force limit of the DREM and investigates if it is numerically accurate.

2. METHODS

2.1. DREM MD Protocol. The DREM simulations of the LZ and bZIP were run with the CUKMODY[48] explicit solvent protein molecular dynamics code. Details of the simulation setup are available for the LZ[31] and for the bZIP.[40] Briefly, for the LZ, with 31 residues in each monomer, the simulations were carried out at 275 K in a box with 59.1851 Å sides, 6377 SPC water molecules, and 2 Cl^- ions, for neutrality, with standard protonation states for all residues. For the bZIP with 57 residues in each monomer, the simulations were carried out at 303 K in a box with a linear dimension of 88.78 Å with 22251 SPC water molecules. With standard protonation states for all of the residues, 15 Cl^- ions were added for neutralization of residues, along with 84 Na^+ and 84 Cl^- ions to approximate 200 mM conditions where the collapsed basic region trajectory was found.[40]

The DREM is implemented by adding to the MD Hamiltonian $H(\mathbf{X},\mathbf{P})$ a window potential $V_i(\mathbf{R})$ (i = 1, 2, ..., N_w) such that $H_i(\mathbf{X},\mathbf{P}) = H(\mathbf{X},\mathbf{P}) + V_i(\mathbf{R})$, where $\mathbf{R} = \mathbf{f}(\mathbf{X})$ denotes a set of restraint coordinates that depend on the configuration, $\mathbf{X}$, and $\mathbf{P}$ denotes the canonical momenta.[48] Between exchange attempts, normal MD is run for each system i characterized by $H_i(\mathbf{X},\mathbf{P})$. When system interchanges are to be attempted, detailed balance

$$\alpha(\mathbf{X}, \mathbf{X}' \rightarrow \mathbf{X}', \mathbf{X})P_i(\mathbf{X})P_j(\mathbf{X}') = \alpha(\mathbf{X}', \mathbf{X} \rightarrow \mathbf{X}, \mathbf{X}')P_i(\mathbf{X}')P_j(\mathbf{X}) \quad (1)$$

must be enforced. Here, $\alpha(\mathbf{X},\mathbf{X}' \rightarrow \mathbf{X}',\mathbf{X})$ is the acceptance probability (transition probability) that configuration $\mathbf{X}$ in the ith system and $\mathbf{X}'$ in the jth system before exchange result in configuration $\mathbf{X}'$ in the ith system and $\mathbf{X}$ in the jth system after exchange, and $P_i(\mathbf{X})$ is the Boltzmann distribution at temperature $T = 1/k_B\beta$ for the ith system. The Metropolis rule for exchange acceptance/rejection between two systems

$$\alpha(\mathbf{X}, \mathbf{X}' \rightarrow \mathbf{X}', \mathbf{X}) = \min(1, e^{-\Delta(\mathbf{X},\mathbf{X}' \rightarrow \mathbf{X}',\mathbf{X})}) \quad (2)$$

where

$$\Delta(\mathbf{X}, \mathbf{X}' \rightarrow \mathbf{X}', \mathbf{X}) = \beta[(V_i(\mathbf{X}') - V_j(\mathbf{X}')) + (V_j(\mathbf{X}) - V_i(\mathbf{X}))] \quad (3)$$

guarantees that Boltzmann equilibrium in the extended ensemble of the product of all of the systems' ensembles will result in a sufficiently long trajectory. If the restraint potential functions differ by a restricted set of degrees of freedom, $\mathbf{R}$, only those will contribute to eq 3.

dx.doi.org/10.1021/jp504723m | J. Phys. Chem. B 2014, 118, 10341−10354

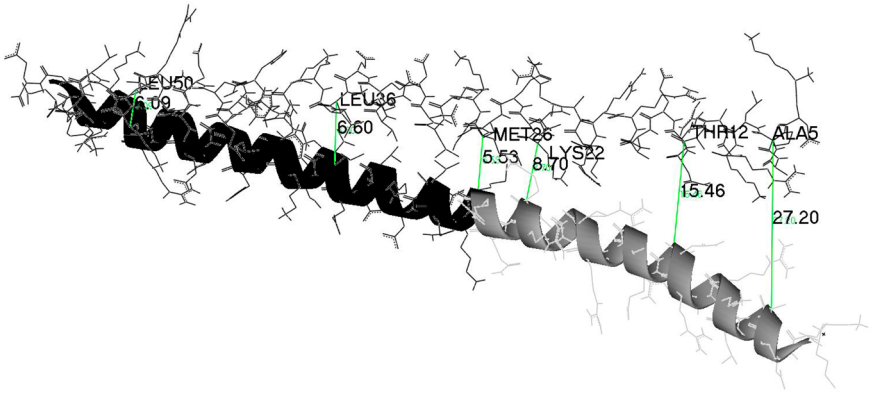

Figure 1. BZIP dimer with the coiled coil in black and the basic region in gray for one monomer. The CA−CA′ monomer-to-monomer′ distances between three basic region (Ala 5, Thr 12, Lys 22) and three coiled coil (Met 26, Leu 36, Leu 50) residues are indicated. The corresponding residues in the LZ are Leu 26 (LZ) = Leu 50 (bZIP), Leu 12 (LZ) = Leu 36 (bZIP), and Met 2 (LZ) = Met 26 (bZIP)).

Because any REM can be viewed as attempted exchanges of parameters (versus exchanges of configurations), if there is a small set of restraint parameters, for example, desired restrained distances and restraint force constants, the method is computationally efficient. Our implementation runs systems independently on different nodes of a Linux cluster computer, and when exchanges are attempted, information is passed using the Message Passing Interface technique implemented as MPICH. In this way, frequent exchange attempts (we typically use every 40 MD steps) can be done without much sacrifice of efficiency.

2.2. Restraint Potentials, WHAM, and Window Overlaps. The restraint potential used in this work has the form

$$V_w(\{r_b^w\}) = \sum_{b=1}^{B} \frac{1}{2} k_b^w (\delta r_b^w)^2$$
$$\delta r_b^w = r_b^w - r_b^{\mathrm{eq},w} \tag{4}$$

with k_b^w and $r_b^{\mathrm{eq},w}$, respectively, the force constant and equilibrium restraint value for "bond" b in window w. Here, for example, the bonds are various atom−atom distances between the two monomers. The sum form of the window restraint potentials permits sampling a variety of individual bond distances but does not permit large deviations from the overall restrained structure.

Let $R = g(\{r_b\})$ denote a scalar reaction coordinate that is given by some function of the restrained coordinates. For obtaining a PMF(R) with this restraint potential, WHAM must be carried out in two steps. First is the iterative determination of the window free energies required to unbias the probability density, and second is construction of the PMF(R) for reaction-coordinate-histogramed values based on the unbiased density.

The window free energies f_w are obtained from solution of[45]

$$\mathrm{e}^{-\beta f_w} = \sum_{w'} \sum_{s} \left[\frac{\mathrm{e}^{-\beta V_w(\{r_{b,s}^{w'}\})}}{\sum_k \mathrm{e}^{-\beta[V_k(\{r_{b,s}^{w'}\}) - f_k]}} \right] \tag{5}$$

where we denote the trajectory snapshots with index s. Note that for a summed bias potential, there is no histogram method for this step because the reaction coordinate does not have a one-to-one relation to the biasing potential; the f_w are functions of the V_w. It is also the case that using an explicit expression in terms of trajectory snapshots for this step is, in general, more accurate than using a histogram method.

Once the f_w are available, the unbiased WHAM probability density is obtained from[45]

$$p^{\mathrm{u}}(R) = \sum_w \sum_s c_{w,s} \eta_s^w(R) \tag{6}$$

where

$$c_{w,s} = \sum_{w'} \mathrm{e}^{-\beta[V_{w'}(\{r_{b,s}^w\}) - f_{w'}]} \tag{7}$$

and

$$\eta_s^w(R) = 1 \quad R < R_s^w < R + \mathrm{d}R$$
$$= 0 \qquad \text{otherwise} \tag{8}$$

bins the reaction coordinate values. The so-obtained, unbiased window probability distributions then provide PMFs according to

$$\mathrm{PMF}(R) = -k_{\mathrm{B}} T \ln\left(\frac{p^{\mathrm{u}}(R)}{p^{\mathrm{u}}(R_{\mathrm{ref}})} \right) \tag{9}$$

with R_{ref} as some reference value.

As noted above, the form of eq 4 for one bond shows that there is a one-to-one relation between energy V_w and bond distance r_b^w. In that case, the degree of overlap of the biased window densities can be used to decide if appropriate window means and variances have been chosen. For the multibond case, the connection between window energies and a coordinate to reflect window histogram overlap is not direct. To obtain such a connection for a potential of the form of eq 4 with more than one restraint coordinate, first define average coordinates

$$\bar{r}^w = \frac{1}{B} \sum_{b=1}^{B} r_b^w \tag{10}$$

and their corresponding deviations from their restrained values

$$\delta \bar{r}^w = \bar{r}^w - \frac{1}{B} \sum_{b=1}^{B} r_b^{\mathrm{eq},w} \tag{11}$$

Then, introduce the potential

dx.doi.org/10.1021/jp504723m | J. Phys. Chem. B 2014, 118, 10341−10354

$$\bar{V}_w(\{r_b^w\}) = \sum_{b=1}^{B} \frac{1}{2} k^w (\delta \bar{r}^w)^2 = \sum_{b=1}^{B} \frac{1}{2B^2} k^w (\delta r_b^w)^2 + \sum_{b=1}^{B} \sum_{b' \neq b}^{B} \frac{1}{2B^2} k^w (\delta r_b^w)(\delta r_{b'}^w) \quad (12)$$

where the force constant values are assumed to be independent of the particular bond, for simplicity. If the second mixed term tends to zero, as it tends to be because the δr_b^w fluctuate around zero, then $\bar{V}_w$ will be a proxy for V_w in eq 4. The overlap of the histograms of the average coordinates $\bar{r}^w$ will then measure the extent to which the WHAM method is accurate.

A simplification of WHAM when the restraint force constants are sufficiently large for this averaged reaction coordinate is given in Appendix A.

2.3. LZ: Details of Bonds and Restraints. The monomers of the LZ dimer simulated consist of 31 residue truncations (the last two residues are not resolved)

a d a d a d a d a

R[MKQLEDK][VEELLSK][NYHLENE][VARLKKL]VG.

of the 33 residue, parallel, two-stranded, LZ GCN4-p1 of the yeast transcriptional activator GCN4. The four heptad (*abcdefg*) repeats are bracketed, and the *a* and *d* positions are indicated in the above sequence. The heptad repeat is the characteristic motif of LZs. The initial LZ coordinates were obtained from a crystal structure[49] (PDB accession code 2ZTA). Figure 1 displays the bZIP dimer, with the LZ subdomain of one monomer indicated in black. The simulated LZ then consists of the black coiled coil and its other corresponding monomer

For reasons given in section 3, the LZ PMF was obtained in three distance ranges. In all of them, three CA−CA′ (monomer−monomer′) distances were used to form the restraint given in eq 4, namely, Leu 5, Asn 16 and Val 23, (indicated in the earlier sequence above in boldface). In all of the ranges, eight windows were used. For the "infra" range, these distances were linearly interpolated between the values (in Å) (5.76, 6.25), (4.61, 5.16), and (4.786, 5.27), respectively. For the "bound" range, they were linearly interpolated between (6.76, 9.24), (5.61, 8.37), and (5.78, 8.24), respectively. For the "separating" range, they were linearly interpolated between (9.95, 12.4), (9.16, 11.9), and (8.94, 11.4), respectively. The force constants used are indicated in Table 1 along with the reaction coordinate ranges covered. The initial coordinates for all three ranges were obtained from a 1 ns eight window DREM simulation that covered the infra to separating ranges.

2.4. bZIP: Details of Bonds and Restraints. The crystal structure of GCN4[4] (PDB accession code 1YSA) without DNA was used to initiate the MD. There are 114 resolved residues in the dimer (the beginning MET in the first monomer and ending ARG in the second monomer were not resolved). Figure 1 displays the bZIP dimer. The basic region CA-CA′ distances that were restrained are of residues Ala 5, Thr 12, and Arg 19. The PMF was run in two ranges, closed to extended and extended to open. The designation closed to extended interpolates between distances (in Å) (5.83, 16.0), (4.97, 12.0), and (3.92, 7.94) for these residues, respectively. The designation extended to open interpolates between distances (16.0, 26.1), (12.0, 18.8), and (7.94, 11.9), respectively. These distances cover an essentially scissors-like motion of the basic region monomer−monomer separation.

Table 1. Summary of LZ Simulations

range	PMF range (Å)	number restraints/FC[a]	histo overlap	exchange
infra	5.5−5.7	3/20	high	none
infra	5.5−5.7	3/40	high	none
bound	5.5−9	3/5	high	0.15−0.28
bound	5.5−9	3/10	moderate	0.05−0.09
separating	9.0−12.5	3/5	moderate, gaps	0.02−0.25

[a]Force constant (FC) in kcal/mol/Å^2.

3. RESULTS FOR THE LZ

The PMF for separating the LZ dimer was run in three distance ranges, with conditions summarized in Table 1. The Alber and co-workers crystal structure[49] that is a pure LZ was used to initiate the MD because the focus in here is on the properties of a LZ versus the LZ domain that is part of a bZIP. The DREM was run using different reaction coordinate ranges due in part to computer resource limitations. Also, the PMF has different characteristics at different distances; for example, to obtain the PMF in a close range where the monomers begin to overlap requires large force constants that are needed to restrain the distances to appropriate ranges. Other things being equal, large force constants can and do produce poor REM behavior (the exchange energy is exponential in the force constants, as is clear from eq 3). Other reaction coordinate ranges can be run with smaller force constants that can cover a larger interval and may lead to larger DREM exchange probabilities.

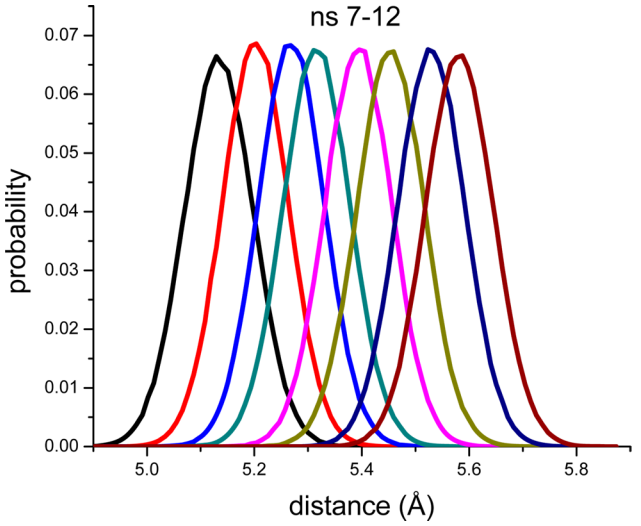

Figure 2. Histograms of the eight biased window densities for the LZ infra reaction coordinate range, with FC = 40 kcal/mol/Å^2.

Each simulation was carried out with a potential that is a sum over the three bond restraints noted in section 2.2 and illustrated in the left part of Figure 1. The summed restraint allows for a certain amount of separation, rotation, and slippage of one monomer relative to the other monomer in each window. The reaction coordinate is the average over these three monomer−monomer distances. Eight windows were used in each PMF range. The three ranges will be referred to as "infra", "bound", and "separating", indicating their character.

dx.doi.org/10.1021/jp504723m | J. Phys. Chem. B 2014, 118, 10341−10354

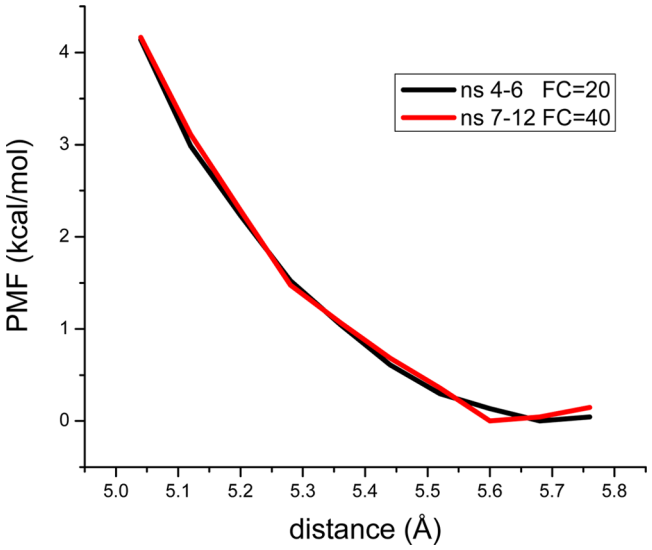

Figure 3. LZ PMF for the infra reaction coordinate range. The PMFs generated with two values of the force constant, 20 and 40 kcal/mol/Å^2, agree well, and convergence to a stable result is rapid.

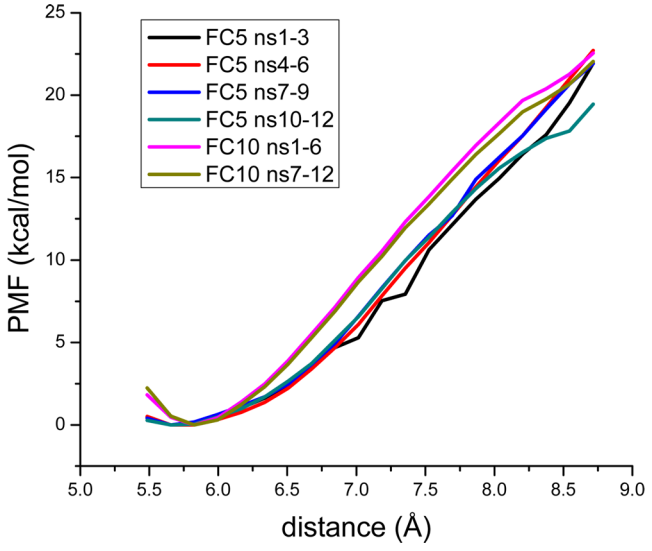

Figure 4. LZ PMF for the bound region for several time intervals and two force constant values.

Table 2. LZ Bound Region[a]

	exchange fraction[b]	
exchange pair	FC = 5[c]	FC = 10[c]
0 ↔ 1	0.278	0.084
2 ↔ 3	0.274	0.083
4 ↔ 5	0.196	0.046
6 ↔ 7	0.161	0.047
1 ↔ 2	0.274	0.095
3 ↔ 4	0.235	0.057
5 ↔ 6	0.154	0.050

[a]Exchange fractions for the two force constant values used. [b]Exchanges were attempted every 40 MD steps. [c]FC (force constant) in kcal/mol/Å^2.

3.1. Infra PMF Is Repulsive. For obtaining the PMF when the monomers are strongly bound into a dimer, to see if they can sample closer than equilibrium distances, strong force

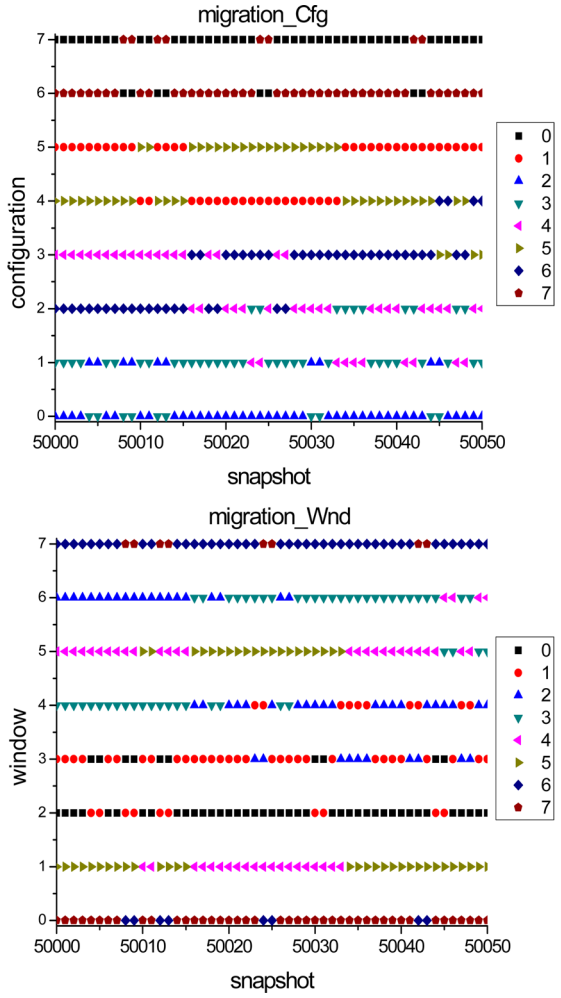

Figure 5. LZ bound range exchange patterns over 50 snapshots for the FC = 5 kcal/mol/Å^2 data. The migration_Cfg plot indicates, for a given configuration (replica), which window (restraint potential) is visiting on that snapshot. The migration_Wnd plot indicates, for a given window (restraint potential), which configuration (replica) is visiting. There is good mixing evident; for example, in migration_Cfg, the seventh replica is mainly occupied by the zeroth window potential.

constants are required. In Figure 2, we display histograms of the biased window densities in the reaction coordinate (the average value of the three distances used for the restraints) that serves as a proxy for window overlap, as discussed in section 2.2, using 40 kcal/mol/Å^2 force constants. Similar results are obtained with 20 kcal/mol/Å^2 force constants.

The PMFs with use of the two force constants are shown in Figure 3 and are essentially identical. The time range is indicated on the figure. Convergence to stable results is relatively rapid. The equilibrium distance of the reaction coordinate is around 5.8 Å based on the crystal structure, and this is closely followed in the PMF.

3.2. Bound PMF Is Very Strongly Associative. The bound region designation refers to the strong "knobs-into-holes"[50] interactions that provide the stability of the LZ dimer. Figure 4 displays the PMF evaluated over different time intervals and for two force constant choices. The agreement among the FC = 5 kcal/mol/Å^2 time intervals is good and compares reasonably well with the FC = 10 kcal/mol/Å^2 results. The main feature is the very deep free-energy well that binds the LZ monomers together. Even when the

dx.doi.org/10.1021/jp504723m | J. Phys. Chem. B 2014, 118, 10341−10354

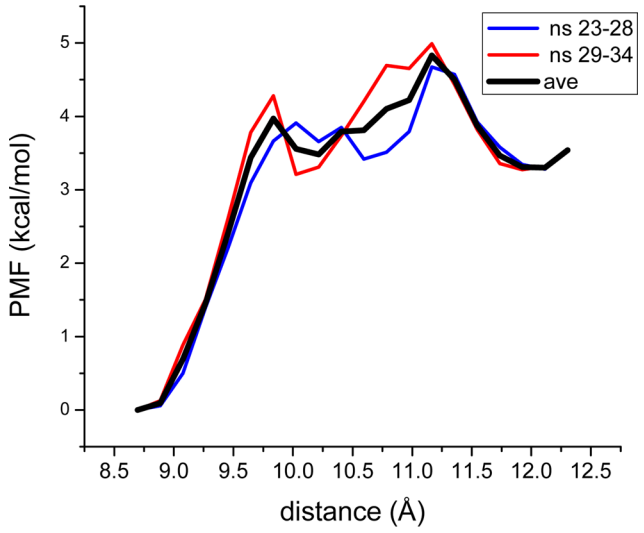

Figure 6. LZ PMF for the exterior region. The convergence is very slow, with earlier intervals progressively decreasing in PMF value at the larger distances from ∼7−8 kcal/mol to the displayed values.

Table 3. LZ Separating Region[a]

	exchange fraction	
exchange pair	23−28 ns	29−34 ns
0 ↔ 1	0.199	0.231
2 ↔ 3	0.170	0.210
4 ↔ 5	0.029	0.091
6 ↔ 7	0.254	0.254
1 ↔ 2	0.099	0.034
3 ↔ 4	0.138	0.115
5 ↔ 6	0.262	0.244

[a]Exchange fractions for two time intervals.

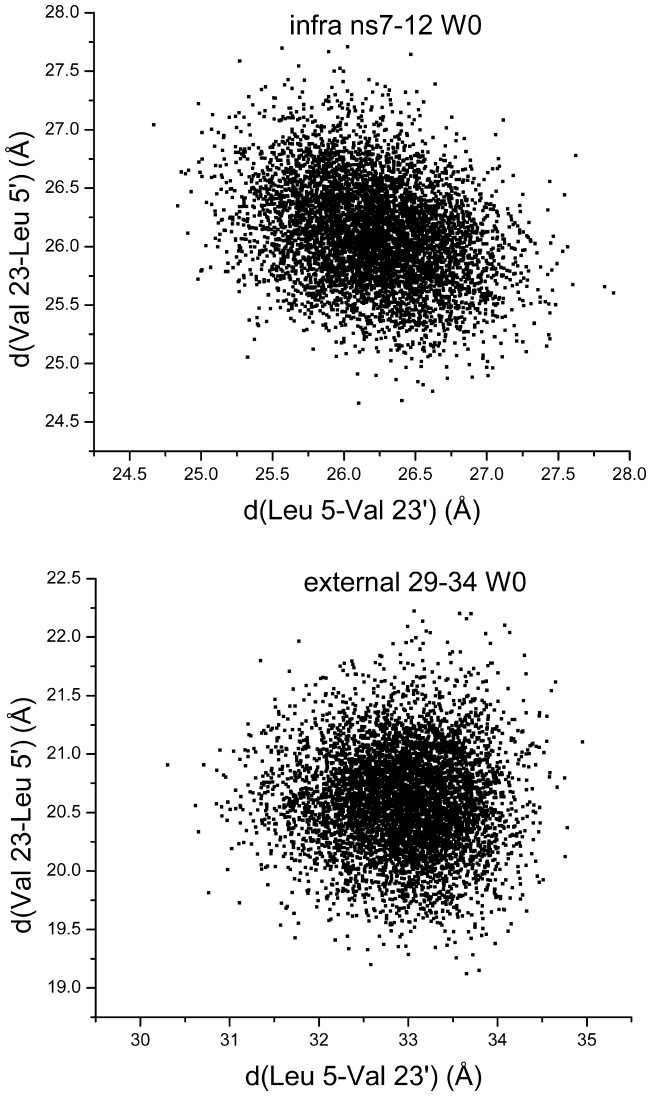

Figure 7. LZ monomer CA−CA′ distances for Leu 5−Val 23′ and Val 23−Leu 5′ in window 0. Data from the infra and external DREM simulations are shown. The distance distributions in each case are unimodal. For the external distance simulation, the two cross distances are different, indicating a displacement of one monomer relative to the other monomer.

monomers are separated by ∼3 Å relative to their equilibrium separation ∼5.7 Å, there is a very strong tendency to capture the monomers.

The PMF changes dramatically in this region owing to the strong forces operating between the monomers. Thus, it is of interest to investigate the quality of the DREM procedure. The overlap of the window densities (data not shown) is excellent, indicating that the restraints are sufficiently large to maintain the desired distances well and cover the desired reaction coordinate range yet still lead to good window overlap.

Table 2 lists the exchange probabilities for the indicated force constants. With exchanges attempted every 40 MD steps, there are 37501 attempts in a 6 ns run, noting that exchanges are alternately attempted with even and odd windows. With the indicated exchange probabilities in Table 2, there are ample successful exchanges that should provide the desired DREM enhanced sampling.

Also important to successful REM sampling is the itineration of the windows (specified by the window potential, V_w) among the configurations and vice versa. Figure 5 displays a short section (for clarity) of these itinerations for the FC = 5 kcal/mol/Å^2 data. Examining the migration_Cfg plot for, for example, configuration 2 on the "configuration" axis as a function of the snapshot index shows that the restraint potential (the window) in operation at a given snaphsot instant is changing as the snapshot changes. For configuration 2, the plot shows that the differing equilibrium distance restraint potentials from the restraints in windows 3, 4, and 6 are sampled. Thus, over this short time interval, configuration 2 is experiencing a variety of different restraint potential distances. It is this feature that is essential in greatly enhancing the configuration space exploration. The other configuration indices show the same feature. Also note that what was initially the window (restraint potential) 0 equilibrium distance (the square dot) has migrated to window 7 in this short interval, indicating the rather rapid "mixing" in this REM. Similar considerations apply to the migration_Wnd plot. Because exchanges are attempted every 80 fs, these plots demonstrate that exchanges occur on a subpicosecond time scale.

3.3. Exterior PMF Levels Off. The PMF for the exterior region, where the forces binding the monomers are weakening, is shown in Figure 6. Two time ranges of 23−28 and 29−34 ns are displayed and averaged. With the approximately 4 kcal/mol increase before leveling off and the ∼20 kcal/mol increase from the bound region, the monomer binding free energy is about 24

dx.doi.org/10.1021/jp504723m | J. Phys. Chem. B 2014, 118, 10341−10354

kcal/mol. In the exterior region, the convergence is quite slow. For earlier 5 ns time intervals, the increase before stabilization falls from ∼7 kcal/mol to the value shown in Figure 6.

The DREM exchange fractions are listed in Table 3 and show that for the most part, the exchange fractions are good. Again, with the frequent exchange attempts, there should not be a problem for convergence arising from the DREM. One possible source for slow convergence could be the sampling of local residue motions. Comparing the RMSFs (root-mean-square fluctuations) of each residue in each monomer between the infra, where convergence was rapid, and this exterior reaction coordinate region shows that both the backbone and all heavy atom RMSFs are quite similar. Thus, local sampling does not seem to be an issue.

However, there are differences in the relative, global motions of the two monomers that are instructive. To investigate this issue, consider "cross" distances between the two monomers, that is, monitoring the Leu 5−Val 23′ and Val 23−Leu 5′ distances will show if there is a slippage between the two monomers. Note that the form of the restraint potential serves as a way of keeping the three monomer−monomer distances in ranges yet allows the monomers to come closer (over part of them). This is in contrast with window restraints that would use three individual distance restraint potentials, whereby the monomers would have to stay lined up. Figure 7 displays data for the infra 7−12 ns time interval that shows that window 0 gives a tight circle for these two cross distances. Therefore, there is no slippage. For the external 29−34 ns window 0, there is slippage (one monomer is shifted relative to the other), but a circle is still obtained, that is, only one "state" is being sampled.

In contrast, Figure 8 shows that the corresponding window 7 data exhibit essentially one state during the earlier time interval (1−4 ns) and two (antidiagonal) states during the later time interval (29−34 ns), indicating that, eventually, there is a large slippage of one monomer relative to the other, in one direction or the other. Furthermore, that is all of the distances that are sampled; there is no slow transition of distances between these extremes.

This must be a consequence of the DREM procedure, where oppositely slipped monomer configurations are sufficiently close in energy that they will exchange, and their weights, as indicated in Figure 8, are more or less the same. Conformations that correspond to these states are displayed in Figure 9. In essence, the long time to convergence in this exterior distance range is most likely due to the forces acting between monomers becoming relatively small as the monomers are separating and the consequential enlargement of the configurational space exploration.

4. RESULTS FOR THE BZIP

The bZIP dimer is composed of a LZ sequence, which produces a stable α-helical coiled coil, and a DNA recognition subdomain (basic region), so-named because it has a great excess of basic residues. Figure 1 displays the bZIP dimer geometry. Residues Gln 24, Arg 25, and Met 26 form a turning point between the coiled coil and the basic region, residues 1−25. Our previous no-restraint MD[40] showed that the basic region monomers could undergo a relative scissors-like motion that was relatively unhindered that, for some trajectories, would spontaneously "collapse" to a close monomer-to-monomer distance conformation. Thus, our interest is in obtaining a PMF for this scissor-like motion. To that end, the restrained basic region residues used in the DREM are Ala 5, Thr 12, and Arg

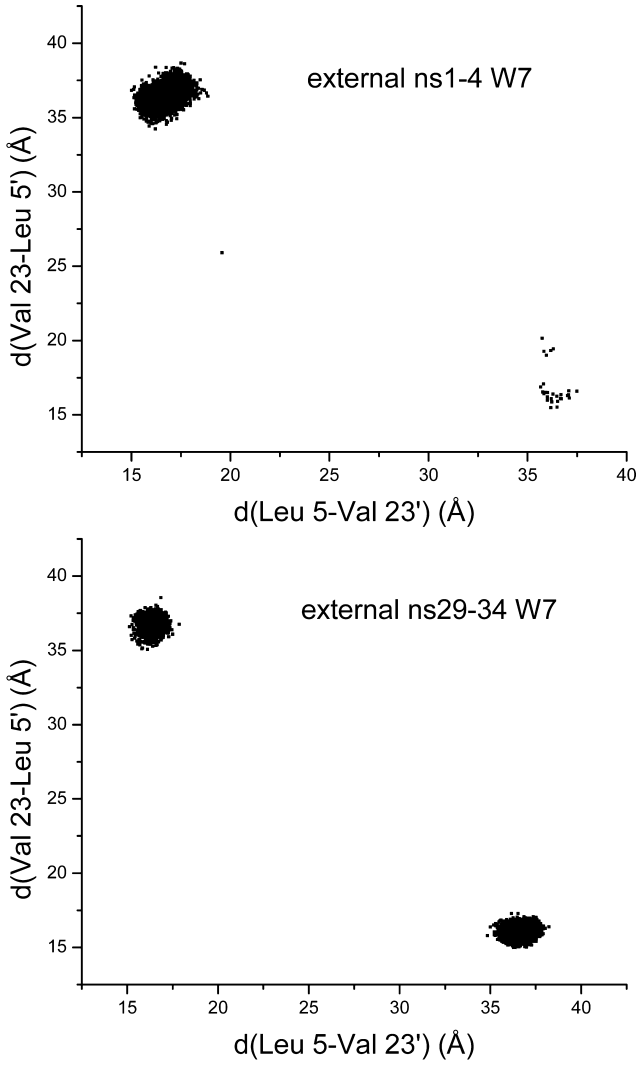

Figure 8. LZ monomer CA−CA′ distances Leu 5−Val 23′ and Val 23−Leu 5′ in window 7 (where the restraint distance is largest) for the external DREM simulation. For the earlier simulation time interval, the two cross distances are different and almost completely maintained for the simulation time. For the later simulation time interval, there are almost equal populations of the two possible cross distances.

19. The same sum of distances potential form as that for the LZ was used for the restraint energy, with some simulations run with three and others with one restraint, on Thr 12. Here, it makes sense to consider PMFs for several intermonomer basic region distances. We always use the three distances whose sum is restrained in the PMF constraint energy. Table 4 summarizes the bZIP simulations, with the distance ranges covered for each restrained residue distance PMF indicated. The PMFs were obtained over two distance ranges, using eight windows in each range. They were run in the directions specified for reasons discussed below.

4.1. Extended to Open PMF Is Flat. When the basic region samples distances where the monomers are well separated, one might anticipate that they are weakly interacting, leading to a rather flat PMF, though energetic arguments do need to be complemented by entropic considerations. The simulations were run in both directions, that is, for the open (completely open) to extended (partially open) run, starting from the open state resulting from MD based on the crystal

dx.doi.org/10.1021/jp504723m | J. Phys. Chem. B 2014, 118, 10341−10354

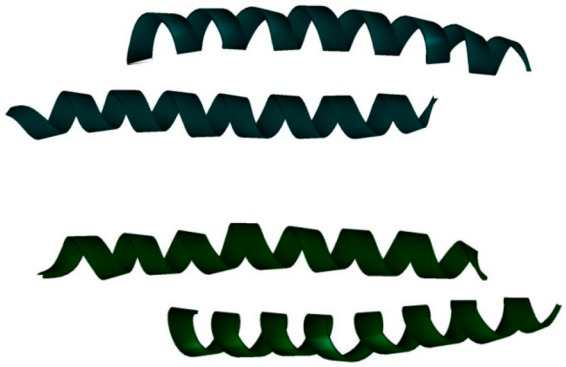

Figure 9. Two conformations of the LZ from the exterior reaction coordinate simulation in window 7 over the 29−34 ns time interval. (Monomer 1 is on top in both conformations.) They illustrate the slippage that produces the different Leu 5−Val 23′ and Val 23−Leu 5′ distances shown in Figure 8. The DREM-based trajectory provides sampling of these very different conformations during this later simulation time interval.

Table 4. Summary of bZIP Simulations

range designation[a]	PMF ranges[b] (Å)	num rest/ FC[c]	histogram overlap	exchange
open to extended	16.0−26.1	3/5	moderate	none
	12.0−18.8			
	7.94−11.9			
extended to open		3/5	moderate	none
closed to extended	5.83−16.0	1/5	high	0.1−0.3
	4.97−12.0			
	3.92−7.94			
closed to extended		3/5	small	none
extended to closed		3/5	small (gaps)	none
extended to closed		1/5	high	0.02−0.07

[a]Open is fully open, extended is partially open, and closed is collapsed (as obtained from a previous simulation). [b]The Ala 5, Thr 12, and Arg 19 CA−CA′ monomer distance ranges, respectively. [c]Number of restraints/force constant (FC) in kcal/mol/Å^2.

structure and covering, with the restraints, to an extended state. This results in the PMF ranges shown in Table 4. Then, starting from this extended state, using the same restraints, it covers the region to the same open state. As noted in Table 4, in both simulation directions, there is good window overlap but essentially zero exchange probability. The three PMFs for monomer−monomer CA separation of residues Ala 5, Thr 12, and Arg 19 are shown in Figures 10−12 for the fourth nanosecond of simulation in both cases. Noting the subthermal (kT = 0.6 kcal/mol at 303 K) variation for Ala 5 and Thr 12 and some slight evidence for structure in the Arg 19 PMF, it appears that the intermonomer basic region fluctuations are essentially unimpeded in this distance regime. Other 1 ns intervals lead to similar results on the scale of thermal fluctuations.

4.2. Closed to Extended PMF Has a Bound State. The PMF for breaking out of the closed state was difficult to obtain for reasons detailed below. Figure 13 shows the PMFs based on starting from the collapsed conformation with the use of one restraint, on Thr 12, the middle restraint of the three. Table 4 notes that the window overlap is high and the exchange probability ranges between 0.1 and 0.3. In this direction, the PMFs show that the collapsed state found from the previous free MD simulation is a stable state, separated from the broad range of essentially noninteracting basic region monomers by about 4−8 kcal/mol dependent on the PMF reaction coordinate. A simulation with the three restraints led to small biased window overlap and no exchanges, with similar shaped PMFs but a somewhat larger magnitude of PMF increase.

A snapshot of a configuration from the window restraint corresponding to the closed state is shown in Figure 14 aligned with that of the collapsed configuration from which the closed to extended simulation was initiated. The overlap is excellent, indicating that in the DREM initiated from the collapsed state, the simulation path for this window reproduces the closed state.

By contrast, a one-restraint simulation started from an extended state conformation, despite good window overlap and small but finite exchange probability (see Table 4), leads to PMFs that monotonically decrease from the closed state. Examination of a snapshot for the window corresponding to the closed state, displayed in Figure 15, shows that a state different than the collapsed state is found. This is the case for both the three-restraint and one-restraint extended to closed simulations that were carried out for sufficient lengths of time (∼15 ns) to stabilize the PMFs. In summary, reversible paths are not obtained with the restraint conditions used here.

5. DISCUSSION

5.1. DREM Features. In this work, PMFs for separating a LZ and for the relative separation of the basic region of a bZIP were obtained by DREM simulations. For the LZ, with its strongly bound dimer, it proved important to introduce a reaction coordinate that could separate the monomers along a somewhat constrained path. For the bZIP, on the basis of a collapsed state, where the basic region is also quite strongly interacting, similar reasoning applied. Therefore, a one-dimensional reaction coordinate, produced by a restraint potential energy that is a sum over selected monomer−monomer distances, proved useful. A virtue of this reaction coordinate is that it is one-dimensional, which greatly limits the number of restraint windows required while at the same time allowing for a reasonable sampling of configuration space because different individual distances can be sampled in a relatively broad range, consonant with the total restraint energy not becoming too large. That is in contrast to introducing separate restraints that would produce a multidimensional reaction coordinate, each of which would separately constrain each distance to a rather narrow range. When a single restraint leads to configuration space coverage similar to that with multiple restaints, a similar PMF will result, as is the case for the closed to extended simulation discussed in section 4.2.

The one-dimensional, multidistance restraint potential in eq 4 does introduce the issue of how to turn the potential energy that appears in the WHAM scheme into a coordinate that can be histogramed to provide a measure of the biased window density overlaps. To accomplish this, we introduced in eq 12 an effective potential for the average distance (over the restrained distances) that should accurately reflect the biased window density overlaps. In this way, the essential requirement of WHAM that the neighbor window biased densities do have some overlap can be verified. To carry out WHAM, it is then essential to use the two-step procedure presented in section 2.2.

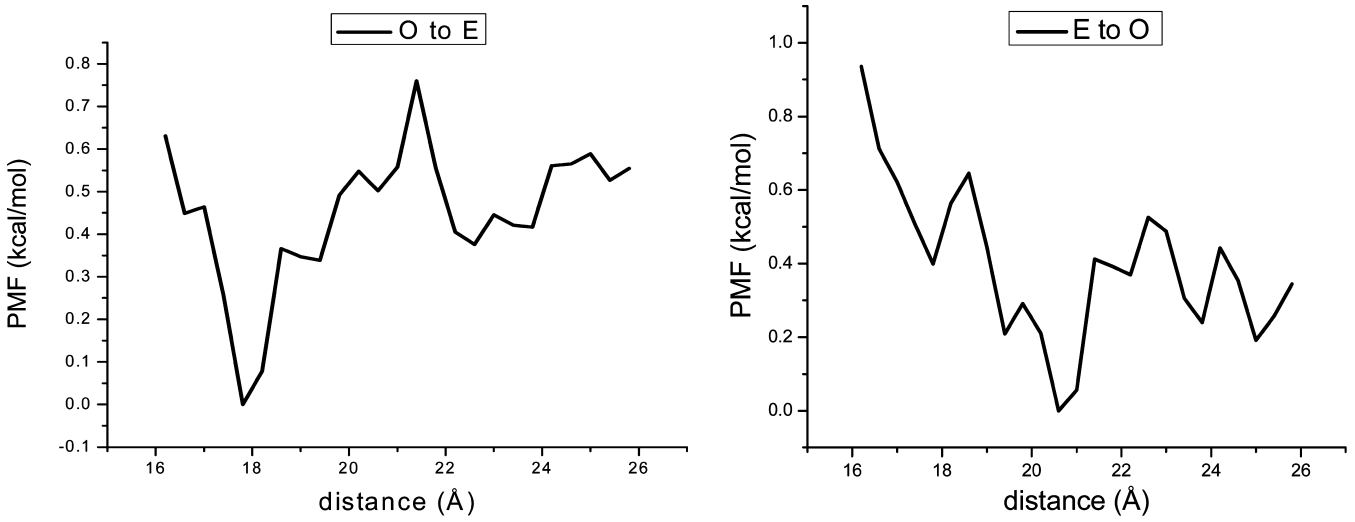

Figure 10. BZIP PMFs for the Ala 5−Ala 5′ CA−CA′ distance from the open to extended (left) and extended to open (right) direction simulations.

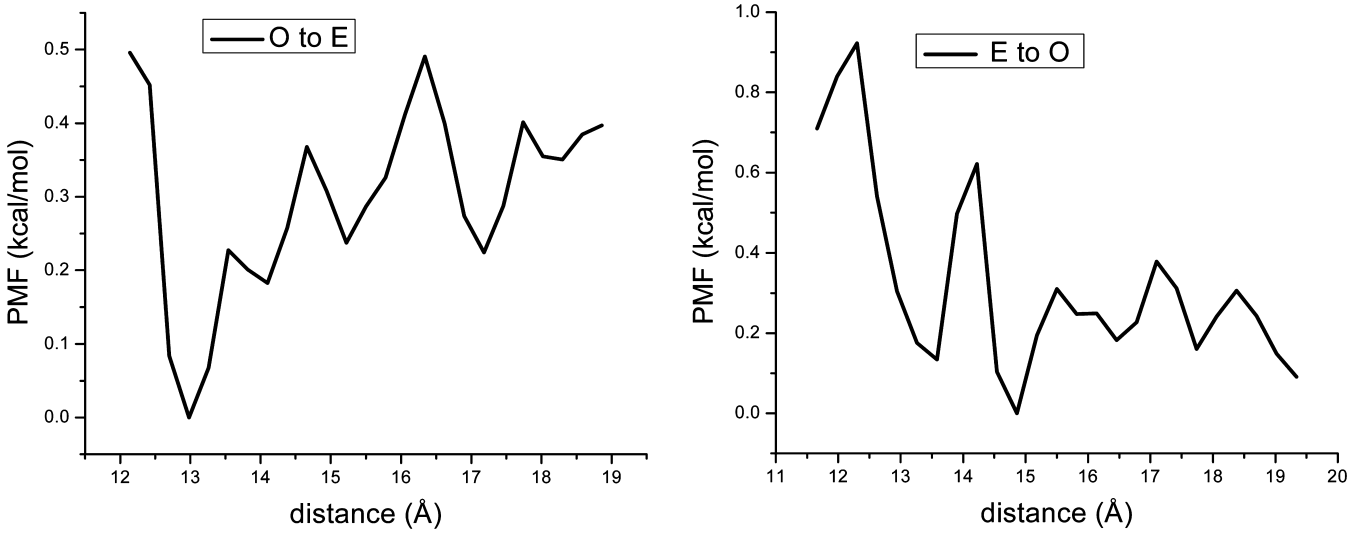

Figure 11. BZIP PMFs for the Thr 12−Thr 12′ CA−CA′ distance from the open to extended (left) and extended to open (right) direction simulations.

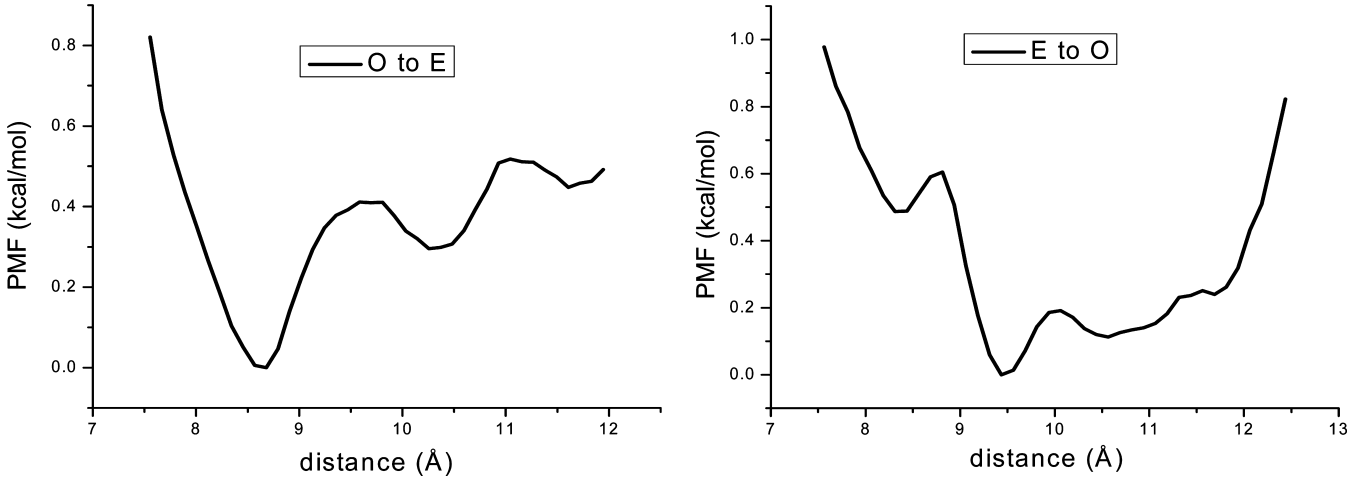

Figure 12. PMFs for the Arg 19−Arg 19′ CA−CA′ distance from the open to extended (left) and extended to open (right) direction simulations.

That is, first iteratively determine the biased window free energies, which depend on the restraint potential values at each window snapshot, as in eq 5. No length scale/histogram is introduced at this step. Then, on whatever desired resolution of

dx.doi.org/10.1021/jp504723m | J. Phys. Chem. B 2014, 118, 10341−10354

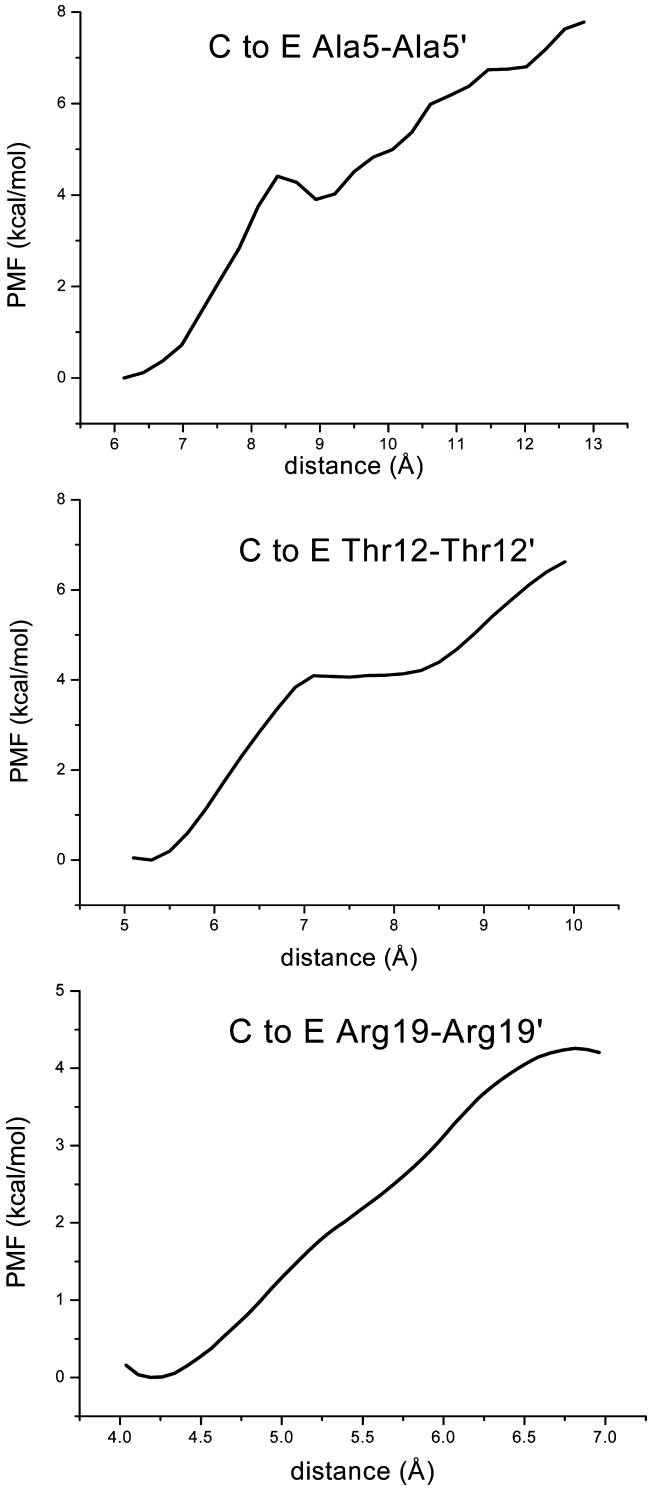

Figure 13. PMFs for binding the bZIP basic region monomers for the indicated three CA−CA′ (see Figure 1) distances that characterize the relative conformation of the basic region monomers for the closed to extended direction simulation.

the reaction coordinate R, the PMF(R) can be determined, as in eqs 6−9, using histograms.

The PMFs were generated in different distance ranges. That is partly an issue of computational resources but also convenient because different distance ranges may require distinctly different force constants and therefore restraint spacings. For a conventional window method (without

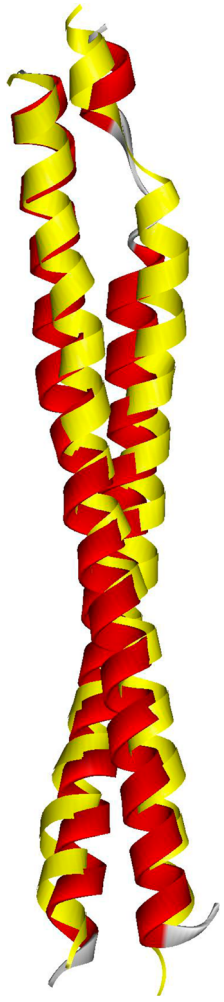

Figure 14. Overlay of the bZIP collapsed starting configuration (red trace) and a snapshot from a one-restraint simulation (yellow trace) in the 12−13 ns. The snapshot is from the window corresponding to the closest distance restraint. The excellent overlay indicates that in the simulation direction from collapsed toward open, the path found is correct.

exchange attempts), that will produce some inefficiency with respect to the region where the two different PMF ranges would be overlapped relative to a set of windows that would cover the entire PMF range. However, it should be noted that, typically, WHAM could equally well be accurately done by obtaining neighbor window pair PMFs and combining all of them to the total PMF. That is evident because while neighbor windows must overlap, usually the next-nearest and farther windows essentially have no overlap.

Running PMFs in ranges for DREM is, in principle, more of an efficiency cost relative to window methods because, for replica exchange, ideally, the entire "ladder" of replicas participates in exchanges. However, DREM can be much more efficient in enhancing sampling than window methods without exchanges because the correlations in a given replica's trajectory can be strongly reduced by exchanges.[48] As in any MC-based method, there is the need to compromise between large move attempts that have poor acceptance and small moves that have good acceptance but do not lead to rapid configurational space exploration. Thus, it proves useful to attempt exchanges often, and therefore, efficient implementation of the exchange attempts is important, as done in

dx.doi.org/10.1021/jp504723m | J. Phys. Chem. B 2014, 118, 10341−10354

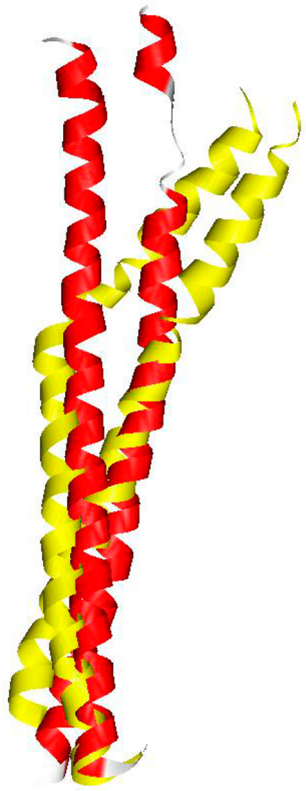

Figure 15. Overlay of the bZIP collapsed starting configuration (red trace) and a snapshot from the simulation in the extended to collapsed direction (yellow trace), using three restraints. The snapshot is from the window corresponding to the closest distance restraint. The closed configuration here is quite different than the collapsed configuration.

CUKMODY. It is also the case that DREM, where the data from all the replicas is explicitly used to construct a PMF, is intrinsically efficient relative to, for example, temperature REM, where typically only the replica corresponding to the ambient temperature has the desired data.

5.2. LZ Is Strongly Bound. The infra PMF range shows that it is repulsive for distances that are smaller than the equilibrium monomer separation of about 5.8 Å, as obtained from the crystal structure. The PMF reaction coordinate is the average over the three restrained CA−CA′ monomer distances used that essentially span the monomer length. In previous simulations,[32] the registry of the backbone and side-chain atoms of the monomers in the dimer was found to be strongly recovered relative to the crystal structure when the monomers were started off from a separation essentially beyond their interaction distance. Thus, this PMF range confirms the minimum distances for the binding free energy and shows that closer separations are repulsive. For this coordinate range, in order to restrain distances, strong force constants were required, and most likely, the PMF is dominated by energy versus entropic factors. As a test of a strong force constant limit of WHAM, as shown in Appendix A, the PMF evaluated at the equilibrium restraint positions (here, with multiple restraints, the average restraint position, $\vec{r}_e^{\,w}$) simplifies to $\mathrm{PMF}(\vec{r}_e^{\,w}) = f_w + c$, with c as a constant setting the zero of energy in the PMF. Thus, the biased potential free-energy parameters f_w would specify the PMF at these points. However, as shown in Figure 16, even for these strong restraint force constants, the strong force constant limit is not reached.

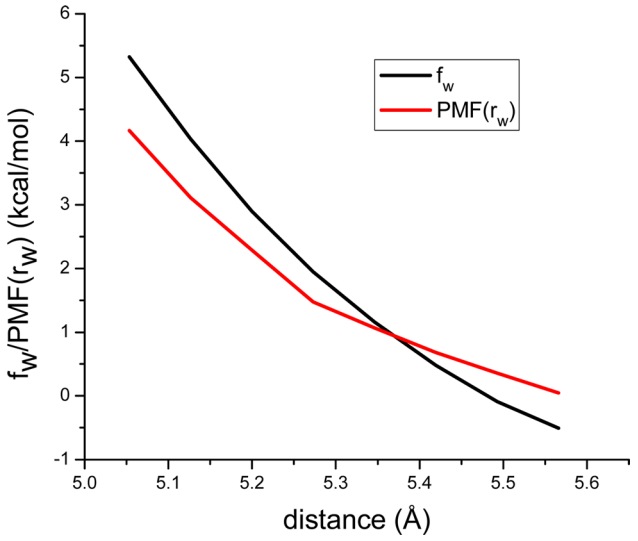

Figure 16. LZ PMF evaluated at the equilibrium window positions compared with the strong restraint force limit result, as discussed in Appendix A. Even for the strong restraint force constant of 40 kcal/mol/Å^2, the strong force limit PMF is not reached.

In the bound PMF range spanning ∼5.8−8.5 Å for the restrained CA−CA′ average distance, the free energy increases by more than 20 kcal/mol (Figure 4). In the exterior region, the PMF additionally increases by about 4 kcal/mol before leveling off (Figure 6). These results indicate a very strongly bound dimer. Because the bound region PMF has such a large dynamic range, the simulations were carried out with different restraint force constants and found to be in good agreement with each other. The exchange fractions (Table 2) should be sufficient for DREM purposes, in view of the frequent exchange attempts, even for the stronger force constant with its smaller exchange fractions. That is supported by the itineration patterns displayed in Figure 5. In this bound range, with its strong forces, the monomers are separating more or less uniformly with some modest amount of slippage, a translation of one monomer relative to the other.

For the exterior region, where the forces are evidently weakening beyond ∼10 Å in the reaction coordinate, a much greater exploration of configuration space comes into play. Most likely, this leads to the slow convergence of more than 25 ns found. Supporting this suggestion are the CA−CA′ monomer distances shown in Figures 7 and 8. At the smaller restraint distance (window 0) for the infra range and at long time (29−34 ns) for the external range, the plots show that one state is being sampled, as monitored by the cross monomer Leu 5−Val 19′ and Val 5−Leu 19′ distances. Note that Figure 7, bottom panel, shows some nonuniform monomer−monomer separation, but it is unimodal, so that only one state is sampled. In contrast, Figure 8 shows similar one-state behavior at short time, but at longer times, for the largest restraint distance (window 7), two more or less equal population, nonuniformly separated states are obtained, as illustrated in Figure 9. In general, the two monomers can slip relative to each other in two similar but opposite configurations. That does require sampling a much larger configuration space than for more uniform separation paths of the monomers.

It is worth noting that to further separate the monomers becomes impractical for these methods. The configuration space of the two monomers grows rapidly with their separation,

dx.doi.org/10.1021/jp504723m | J. Phys. Chem. B 2014, 118, 10341−10354

and also, explicit solvent simulations become impractical. However, once the monomers are separated, the issue becomes one of the entropy of either two rod-like molecules (that can be analytically estimated) or essentially a protein unfolding problem, if there is a helix to random coil transition for the monomers. Thus, the range of monomer−monomer distances that correspond to their interaction distances, as studied here, is the appropriate distance range to simulate.

5.3. bZIP Basic Region Broadly Fluctuates. The LZ subdomain of bZIP is responsible for maintaining the bZIP monomers as a dimer. The monomer−monomer distance fluctuations of the basic region subdomain are then of a limited range and do not present the dissociation issues just discussed for the LZ. PMFs are obtained for three CA−CA′ distances along the basic region (see Figure 1). Note that the restraints may or may not correspond to the PMF coordinates. In general, that can be a source of difficulty if the restrained coordinates do not provide good sampling along the PMF coordinates. For the restraints used here, the PMF coordinates should be well sampled too.

The PMFs for the three distances, Ala 5−Ala 5′, Thr 12−Thr 12′, and Arg 19−Arg 19′, shown in Figures 10−12, are all essentially thermal. For other time intervals, they all show similar "random" fluctuations. Thus, for this distance range, there does not seem to be much impediment to sampling a large conformational space on the basis of either energy (the intermonomer interactions are small) or, as shown by the PMFs, free energies, with their entropic contributions. In the crystal structure, obtained with DNA present, these three distances (Figure 1) are, respectively, 27.2, 15.5, and 8.7 Å. Therefore, in this range, the basic region should be primed for DNA trapping.

For closer monomer−monomer separations, a difference in the PMFs was found when carrying out the simulation in the closed to extended versus extended to closed directions. Of course, in principle, PMF simulations should correspond to reversible paths. The closed state used to initiate the DREM was taken from a previous no restraint set of simulations (each of about 50 ns duration), one of which produced the collapsed state. In this state, shown in Figure 14, the basic region has come within interaction distances of its monomers. Initiating the DREM simulation from the collapsed state does maintain the closed state in the restraint window with parameters closest to the collapsed state. The PMFs for separating from closed to extended shown in Figure 13 indicate that the collapsed state is quite bound. Thus, collapsed states should be more stable relative to states sampled farther out that correspond to rapidly fluctuating configurations. The simulations in the extended to closed direction follow a different path than that of the closed to extended direction. While the restraints are the same in either simulation direction, a representative state from the restraint window with parameters corresponding to the closed state (Figure 15) is clearly not like the closed state. A difficulty with monomer-to-monomer distance restraints is the possibility of large differences in absolute orientation, even if the distances are properly restrained. That seems to be the case here.

6. CONCLUSIONS

Both the leucine zipper (LZ) and the LZ subdomain of the basic LZ are strongly bound to form a dimer. Obtaining a PMF to characterize their stability using MD simulation is therefore a difficult computational task. The use of a distance REM (DREM) can provide sampling along a carefully chosen reaction coordinate. The potential energy restraint introduced here offers a compromise foe computational expense because it is one-dimensional, yet it does allow for sampling a relatively large conformational space, at least for monomer separations that are not too large. The method should be of general utility when it is advantageous to use multiple restraints. The use of this form of restraint does require a two-step procedure in the implementation of WHAM to unbias the restrained windows. Also, a criterion for biased window density overlap has to be formulated in an approximate way as the one-to-one relation between the restraint potential and reaction coordinate is lost. A caution with the use of multiple distance restraints is that while they will produce desired restrained distances, with sufficiently large force constants, desired orientations may not be properly captured and may not produce a desired end point conformation for the PMF.

For the LZ, the PMF for separating to distances where the monomer interaction should be negligible provides a binding free energy of about 25 kcal/mol. For bZIP, the LZ subdomain maintains the dimerized state while the basic region fluctuates thermally over a broad range of relative distances. For closer separations of the basic region monomers, there is the possibility of also dimerizing this region, with a modest binding free energy. That the basic region monomers essentially freely sample a broad range of relative distances may be advantageous for binding DNA, in the sense of a conformational selection mechanism.

APPENDIX A. PMF FOR THE LARGE RESTRAINT POTENTIAL LIMIT

The (biased potential) free-energy parameters f_w obtained in WHAM can be related to the PMF evaluated at the corresponding window positions when the restraint potential is sufficiently large that the width sampled is small compared with the scale of variation of the PMF. For these purposes, again, it is necessary to introduce the average reaction coordinate deviation, as defined in eq 11, that is some function of configuration $\mathbf{X}$. Denote the system potential in the absence of restraints as $V(\mathbf{X})$. For this average reaction coordinate, the biased free energies and PMFs are related according to

$$\begin{aligned} e^{-\beta f_w} &= \int d\mathbf{X}\, e^{-\beta V(\mathbf{X})} e^{-\beta \bar{V}(\delta \bar{r}^w)} \\ &= \int d\mathbf{X}\, [\int dR\, \delta(R - \delta \bar{r}^w)] e^{-\beta V(\mathbf{X})} e^{-\beta \bar{V}(\delta \bar{r}^w)} \\ &= \int dR\, [\int d\mathbf{X}\, \delta(R - \delta \bar{r}^w) e^{-\beta V(\mathbf{X})}] e^{-\beta \bar{V}(\delta \bar{r}^w)} \\ &= \int dR\, e^{-\beta \mathrm{PMF}(R)} e^{-\beta \bar{V}(R - \bar{r}_e^w)} \end{aligned} \tag{A.1}$$

To the extent that the force constant is large enough to restrain the sampling of R to a small region around $\bar{r}_e^w$, then

$$e^{-\beta f_w} = \int dR\, e^{-\beta \mathrm{PMF}(R)} e^{-\beta \bar{V}(R - \bar{r}_e^w)} \approx e^{-\beta \mathrm{PMF}(\bar{r}_e^w)} \tag{A.2}$$

and

$$\mathrm{PMF}(\bar{r}_e^w) = f_w + c \tag{A.3}$$

with c as a constant. Thus, the biased free-energy parameters coincide with the PMF evaluated at these restraint distances.

dx.doi.org/10.1021/jp504723m | J. Phys. Chem. B 2014, 118, 10341−10354

AUTHOR INFORMATION

Corresponding Author

*E-mail: cukier@chemistry.msu.edu. Phone: 517-355-9715, ext. 263. Fax: 517-353-1793.

Notes

The authors declare no competing financial interest.

REFERENCES

(1) Latchman, D. S. Transcription Factors: An Overview. *Int. J. Biochem. Cell Biol.* **1997**, *29*, 1305−1312.
(2) Miller, M. The Importance of Being Flexible: The Case of Basic Region Leucine Zipper Transcriptional Regulators. *Curr. Protein Pept. Sci.* **2009**, *10*, 244−269.
(3) Vinson, C.; Myakishev, M.; Acharya, A.; Mir, A. A.; Moll, J. R.; Bonovich, M. Classification of Human B-Zip Proteins Based on Dimerization Properties. *Mol. Cell. Biol.* **2002**, *22*, 6321−6335.
(4) Ellenberger, T. E.; Brandl, C. J.; Struhl, K.; Harrison, S. C. The GCN4 Basic Region Leucine Zipper Binds DNA as a Dimer of Uninterrupted Alpha-Helices — Crystal-Structure of the Protein−DNA Complex. *Cell* **1992**, *71*, 1223−1237.
(5) Brandon, C.; Tooze, J. *Introduction to Protein Structure*, 2nd ed.; Garland Publishing: New York, 1999.
(6) Ellenberger, T. Getting a Grip on DNA Recognition: Structures of the Basic Region Leucine Zipper, and the Basic Region Helix-Loop-Helix DNA-Binding Domains. *Curr. Opin. Struct. Biol.* **2004**, *4*, 12−21.
(7) Gruber, M.; Lupas, A. N. Historical Review: Another 50th Anniversary ■ New Periodicities in Coiled Coils. *Trends Biochem. Sci.* **2003**, *28*, 679−685.
(8) Ibarra-Molero, B.; Zitzewitz, J. A.; Matthews, C. R. Salt-Bridges Can Stabilize but Do Not Accelerate the Folding of the Homodimeric Coiled-Coil Peptide GCN4-P1. *J. Mol. Biol.* **2004**, *336*, 989−996.
(9) Lupas, A. N.; Gruber, M. The Structure of Alpha-Helical Coiled Coils. *Adv. Protein Chem.* **2005**, *70*, 37−38.
(10) Marti, D. N.; Bosshard, H. R. Electrostatic Interactions in Leucine Zippers: Thermodynamic Analysis of the Contributions of Glu and His Residues and the Effect of Mutating Salt Bridges. *J. Mol. Biol.* **2003**, *330*, 621−637.
(11) Mason, J. M.; Arndt, K. M. Coiled Coil Domains: Stability, Specificity, and Biological Implications. *ChemBioChem* **2004**, *5*, 170−176.
(12) Matousek, W. M.; Ciani, B.; Fitch, C. A.; Garcia-Moreno, B.; Kammerer, R. A.; Alexandrescu, A. T. Electrostatic Contributions to the Stability of the GCN4 Leucine Zipper Structure. *J. Mol. Biol.* **2007**, *374*, 206−219.
(13) Steinmetz, M. O.; Jelesarov, I.; Matousek, W. M.; Honnappa, S.; Jahnke, W.; Missimer, J. H.; Frank, S.; Alexandrescu, A. T.; Kammerer, R. A. Molecular Basis of Coiled-Coil Formation. *Proc. Natl. Acad. Sci. U.S.A.* **2007**, *104*, 7062−7067.
(14) Woolfson, D. N. The Design of Coiled-Coil Structures and Assemblies. *Adv. Protein Chem.* **2005**, *70*, 80−106.
(15) Bunagan, M. R.; Cristian, L.; DeGrado, W. F.; Gai, F. Truncation of a Cross-Linked GCN4-P1 Coiled Coil Leads to Ultrafast Folding. *Biochemistry* **2006**, *45*, 10981−10986.
(16) Dragan, A. I.; Privalov, P. L. Unfolding of a Leucine Zipper Is Not a Simple Two-State Transition. *J. Mol. Biol.* **2002**, *321*, 891−908.
(17) Meisner, W. K.; Sosnick, T. R. Barrier-Limited, Microsecond Folding of a Stable Protein Measured with Hydrogen Exchange: Implications for Downhill Folding. *Proc. Natl. Acad. Sci. U.S.A.* **2004**, *101*, 15639−15644.
(18) Meisner, W. K.; Sosnick, T. R. Fast Folding of a Helical Protein Initiated by the Collision of Unstructured Chains. *Proc. Natl. Acad. Sci. U.S.A.* **2004**, *101*, 13478−13482.
(19) Nikolaev, Y.; Pervushin, K. NMR Spin State Exchange Spectroscopy Reveals Equilibrium of Two Distinct Conformations of Leucine Zipper GCN4 in Solution. *J. Am. Chem. Soc.* **2007**, *129*, 6461−6469.
(20) Liu, Y.; Chagagain, P. P.; Parra, J. L.; Gerstman, B. S. Lattice Model Simulation of Interchain Protein Interactions and the Folding Dynamics and Dimerization of the GCN4 Leucine Zipper. *J. Chem. Phys.* **2008**, *128*, 045106.
(21) Mohanty, D.; Kolinski, A.; Skolnick, J. De Novo Simulations of the Folding Thermodynamics of the GCN4 Leucine Zipper. *Biophys. J.* **1999**, *77*, 54−69.
(22) Vieth, M.; Kolinski, A.; Brooks, C. L.; Skolnick, J. Prediction of the Folding Pathways and Structure of the GCN4 Leucine-Zipper. *J. Mol. Biol.* **1994**, *237*, 361−367.
(23) Vinals, J.; Kolinski, A.; Skolnick, J. Numerical Study of the Entropy Loss of Dimerization and the Folding Thermodynamics of the GCN4 Leucine Zipper. *Biophys. J.* **2002**, *83*, 2801−2811.
(24) Rojas, A. V.; Liwo, A.; Scheraga, H. A. Molecular Dynamics with the United-Residue Force Field: Ab Initio Folding Simulations of Multichain Proteins. *J. Phys. Chem. B* **2007**, *111*, 293−309.
(25) Choi, Y. H.; Yang, C. H.; Kim, H. W.; Jung, S. Leucine Zipper as a Fine Tuner for the DNA Binding; Revisited with Molecular Dynamics Simulation of the Fos-Jun Bzip Complex. *Bull. Korean Chem. Soc.* **1999**, *20*, 1319−1322.
(26) Yadav, M. K.; Leman, L. J.; Price, D. J.; Brooks, C. L.; Stout, C. D.; Ghadiri, M. R. Coiled Coils at the Edge of Configurational Heterogeneity. Structural Analyses of Parallel and Antiparallel Homotetrameric Coiled Coils Reveal Configurational Sensitivity to a Single Solvent-Exposed Amino Acid Substitution. *Biochemistry* **2006**, *45*, 4463−4473.
(27) Gorfe, A. A.; Ferrara, P.; Caflisch, A.; Marti, D. N.; Bosshard, H. R.; Jelesarov, I. Calculation of Protein Ionization Equilibria with Conformational Sampling: pK_a of a Model Leucine Zipper, GCN4 and Barnase. *Proteins: Struct., Funct., Genet.* **2002**, *46*, 41−60.
(28) Missimer, J. H.; Steinmetz, M. O.; Jahnke, W.; Winkler, F. K.; van Gunsteren, W. F.; Daura, X. Molecular-Dynamics Simulations of C- and N-Terminal Peptide Derivatives of GCN4-P1 in Aqueous Solution. *Chem. Biodiversity* **2005**, *2*, 1086−1104.
(29) Pinero, A.; Villa, A.; Vagt, T.; Koksch, B.; Mark, A. E. A Molecular Dynamics Study of the Formation, Stability, and Oligomerization State of Two Designed Coiled Coils: Possibilities and Limitations. *Biophys. J.* **2005**, *89*, 3701−3713.
(30) Moutevelis, E.; Woolfson, D. N. A Periodic Table of Coiled-Coil Protein Structures. *J. Mol. Biol.* **2009**, *385*, 726−732.
(31) Su, L.; Cukier, R. I. Hamiltonian Replica Exchange Method Studies of a Leucine Zipper Dimer. *J. Phys. Chem. B* **2009**, *113*, 9595−9605.
(32) Cukier, R. I. A Hamiltonian Replica Replica Exchange Method for Building Protein−Protein Interfaces Applied to a Leucine Zipper. *J. Chem. Phys.* **2011**, *134*, 045104.
(33) Bracken, C.; Carr, P. A.; Cavanagh, J.; Palmer, A. G. Temperature Dependence of Intramolecular Dynamics of the Basic Leucine Zipper of GCN4: Implications for the Entropy of Association with DNA. *J. Mol. Biol.* **1999**, *285*, 2133−2146.
(34) Columbus, L.; Hubbell, W. L. Mapping Backbone Dynamics in Solution with Site-Directed Spin Labeling: GCN4−58 bZip Free and Bound to DNA. *Biochemistry* **2004**, *43*, 7273−7287.
(35) Hollenbeck, J. J.; McClain, D. L.; Oakley, M. G. The Role of Helix Stabilizing Residues in GCN4 Basic Region Folding and DNA Binding. *Protein Sci.* **2002**, *11*, 2740−2747.
(36) Saudek, V.; Pasley, H. S.; Gibson, T.; Gausepohl, H.; Frank, R.; Pastore, A. Solution Structure of the Basic Region from the Transcriptional Activator GCN4. *Biochemistry* **1991**, *30*, 1310−1317.
(37) Saudek, V.; Pastore, A.; Morelli, M. A. C.; Frank, R.; Gausepohl, H.; Gibson, T.; Weih, F.; Roesch, P. Solution Structure of the DNA-Binding Domain of the Yeast Transcriptional Activator Protein GCN4. *Protein Eng.* **1990**, *4*, 3−10.
(38) Weiss, M. A.; Ellenberger, T.; Wobbe, C. R.; Lee, J. P.; Harrison, S. C.; Struhl, K. Folding Transition in the DNA-Binding Domain of GCN4 on Specific Binding to DNA. *Nature* **1990**, *347*, 575−578.
(39) Podust, L. M.; Krezel, A. M.; Kim, Y. Crystal Structure of the Ccaat Box/Enhancer-Binding Protein Beta Activating Transcription Factor-4 Basic Leucine Zipper Heterodimer in the Absence of DNA. *J. Biol. Chem.* **2001**, *276*, 505−513.

(40) Cukier, R. I. Simulations of Temperature and Salt Concentration Effects on bZip, a Basic Region Leucine Zipper. *J. Phys. Chem. B* **2012**, *116*, 6071−6086.
(41) Frenkel, D.; Smit, B. *Understanding Molecular Simulation: From Algorithms to Applications*; Academic: San Diego, CA, 1996.
(42) Torrie, G. M.; Valleau, J. P. Monte Carlo Free Energy Estimates Using Non-Boltzmann Sampling: Application to the Sub-Critical Lennard-Jones Fluid. *Chem. Phys. Lett.* **1974**, *28*, 578−581.
(43) Ferrenberg, A. M.; Swendsen, R. H. Optimized Monte-Carlo Data-Analysis. *Phys. Rev. Lett.* **1989**, *63*, 1195−1198.
(44) Kumar, S.; Bouzida, D.; Swendsen, R. H.; Kollman, P. A.; Rosenberg, J. M. The Weighted Histogram Analysis Method for Free-Energy Calculations on Biomolecules. 1. The Method. *J. Comput. Chem.* **1992**, *13*, 1011−1021.
(45) Souaille, M.; Roux, B. Extension to the Weighted Histogram Analysis Method: Combining Umbrella Sampling with Free Energy Calculations. *Comput. Phys. Commun.* **2001**, *135*, 40−57.
(46) Swendsen, R. H.; Wang, J. S. Replica Monte-Carlo Simulation of Spin-Glasses. *Phys. Rev. Lett.* **1986**, *57*, 2607−2609.
(47) Sugita, Y.; Kitao, A.; Okamoto, Y. Multidimensional Replica-Exchange Method for Free-Energy Calculations. *J. Chem. Phys.* **2000**, *113*, 6042−6051.
(48) Lou, H. F.; Cukier, R. I. Molecular Dynamics of Apo-Adenylate Kinase: A Distance Replica Exchange Method for the Free Energy of Conformational Fluctuations. *J. Phys. Chem. B* **2006**, *110*, 24121−24137.
(49) O'Shea, E. K.; Klemm, J. D.; Kim, P. S.; Alber, T. X-ray Structure of the GCN4 Leucine Zipper, a 2-Stranded, Parallel Coiled Coil. *Science* **1991**, *254*, 539−544.
(50) Crick, F. H. C. The Packing of Alpha-Helices — Simple Coiled-Coils. *Acta Crystallogr.* **1953**, *6*, 689−697.